Analysis of interior rotor for high-speed brushless DC motor using finite element method

Nurfaezah Abdullah[1,2], Kasrul Abdul Karim[1,2], Raja Nor Firdaus Raja Othman[1,2], Auzani Jidin[1,2], Tole Sutikno[3,4]

[1]Faculty of Electrical Engineering, Technical University Malaysia Melaka, Melaka, Malaysia
[2]Electrical Machine Design Research Laboratory, Centre of Robotics and Automation, University Malaysia Melaka, Melaka, Malaysia
[3]Master Program of Electrical Engineering, Faculty of Industrial Technology, Universitas Ahmad Dahlan, Yogyakarta, Indonesia
[4]Embedded System and Power Electronics Research Group, Yogyakarta, Indonesia

Article Info	ABSTRACT
	The permanent magnet of brushless DC (BLDC) motor is ideally suited for high-speed application due to its superior performance and efficient as compared to other types of electrical motors. However, to operate in high-speed operation, the rotors that hold the magnet must be able to withstand high centrifugal force. Due to that, the main objective of this project is to design and develop the suitable rotor for high-speed BLDC motor through the finite element method (FEM) Ansys Maxwell modeling software. In addition, this project is also carried out to determine the ability of the modeled software to reach the high-speed performances in terms of cogging torque and induce voltage. In this project, the selected BLDC motor was fabricated and measured experimentally. The result showed that the designed rotor can achieve speed of almost 14,500 rpm.

Corresponding Author:

Kasrul Abdul Karim
Faculty of Electrical Engineering, Technical University Malaysia Melaka
Hang Tuah Jaya, 76100 Durian Tunggal, Melaka, Malaysia
Email: kasrul@utem.edu.my

1. INTRODUCTION

The brushless DC (BLDC) motor has long established in typical applications, such as home appliances, the healthcare industry, air conditioning systems and aerospace systems, especially when an efficient system is required. It is optioned due to its broad uses and advantages, such as high efficiency, high reliability, and low-cost factor. It also has a higher power output that produces better performance and is smaller size compared to other conventional medium or low-speed electrical machines. These factors have led to extensive study in recent years by experts and researchers [1], [2]. Next, the BLDC motors are extensively built for various industrial applications, such as compressors, vacuum pumps, grinders, turbine generators, flywheel energy storage systems, drilling, aerospace application and friction welding units as well [3]–[5]. The centrifugal compressors that are usually used as the loads for motors operation will achieve efficiency of energy and high-power density when they are operated at high speed [6]. In the early years, when electric motors are unable to work at high speed, the boosting gearboxes are required to connect motors and loads. This condition caused a few problems like an extra power loss, affecting the weight and size, producing vibration, and leading to noisy sound. The installation requirements are essential, probable leak of lubricants and a shorter service life. Oppositely, the gearbox can be disabled. For instance, the micro gas turbines used in power plants may drive an average speed of electrical generators with fewer loads to prevent unnecessary breakdown caused [6].

There are several varieties of BLDC motor topologies, including traditional surface mounted (SPM) and inner permanent magnet (IPM). In comparison to the IPM topology, the SPM topology is simpler. The magnet configuration distinguishes these two-topology motors from IPM and SPM. The SPM structures are made up of a stator and a magnet connected to the outside of the rotor, whereas the IPM has an embedded magnet buried in the rotor laminations. Figure 1 depicts the BLDC motor basic rotor arrangement. Figure 1(a) show the surface mount magnet, Figure 1(b) is inset magnet motor type and Figure 1(c) is interior magnet type. The surface mount magnet configuration is the most common for permanent magnet motors, with a magnet located on the outer surface of the rotor core. However, this design is vulnerable to high centrifugal force, which might lead to catastrophic failure [7]–[9]. An interior magnet rotor is a feasible alternative that should be researched further to resolve this [10], [11]. The inner rotor is suitable for a wide range of driving techniques and tactics [12], [13]. Several works of literature, notably for rotor design, emphasize the mechanical issue. Hao *et al.* used the same parameter simulation to examine five inside permanent magnet machine topologies for a hybrid electric automobile, including input voltage, slot and pole number, and motor dimension. The regular PM rotor, segmented PM rotor, V-shaped PM rotor, and W-shaped rotor were all compared. The most important aspect to consider is performance, which includes back-emf harmonics, iron losses and torque ripple. The goal is to provide a preliminary guideline and evaluation to the machine designer in allowing to enable them to select the IPM rotor structure. According to the results, V-shaped PM rotors had the lowest magnet mass. The W-shaped had the highest d-q axis inductance, while the SPM had the lowest. Nonetheless, this modeling was meant for 2,000 rpm [14].
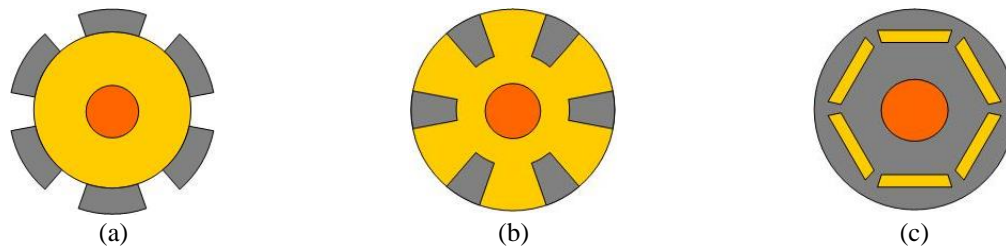

Figure 1. Basic rotor configuration for BLDC motor: (a) surface mounted magnet, (b) inset magnet, and (c) interior magnet

Hao *et al.* conducted research on several rotor topologies for high-speed electrical machines. The research compared the performance of five topologies: bread loaf, decentered magnet, spoke type, surface mounted, and interior permanent magnet in terms of magnetic flux density, cogging torque, torque and efficiency. The Taguchi technique was used to establish the modeling, which was simulated by using FEA. The goal of this research was to identify which topologies can provide high output power, torque, and efficiency for high-speed spindle machines. The decentered permanent magnet motor produced the maximum magnetic flux density, output power and efficiency. This comparison, however, had utilized permanent magnet synchronous motors for high-speed spindle machines rather than IPM-BLDC motors [14].

Purwanto *et al.* investigated the effects of machine structure on PM BLDC motors for high-speed applications. Three distinct slots were present, and the rotor pole model with surface-mounted topology was discussed. The goal of these investigations was to determine the best slot and rotor pole combination for high-speed machines with the best dynamic performance. The authors used 2-pole 6-slot, 2-pole 12-slot and 2-pole 3-slot. The results of this research demonstrated that the 2-pole 12-slot construction had the best electromagnetic properties, while the 2-pole 6-slot motor structure is suited for high-speed dynamic operation. However, the purpose of this research is to investigate the best slot and pole for high-speed dynamic operation [15].

Hwang *et al.* published another paper that looked at different rotor structures. Five IPM rotor structures for electric car applications were studied throughout the project. The modelling included the V shape type, interior double magnet shape, a delta shape including V form magnet bar, improved delta shape model and double V shape. JMAG finite element analysis was used to simulate the design to analyze the electromagnetic torque, torque ripples, efficiency, and back-electromagnetic voltage. The goal of this inquiry is to propose a design standard for rotor forms because there have been few complete investigations on IPM rotor shapes designed for EV use. Another goal of the article is to minimize design and analysis time throughout the design stage to obtain maximum power density. According to the findings of this article, the

delta form had the most torque than other models. Nonetheless, this material is valid for speeds ranging from 5,000 rpm to 10,000 rpm. Aside from that, the modelling is for 48-slot, 8-pole IPM motors [16].

Comparative investigations of internal permanent magnet synchronous motors (IPMSM) for high-speed railway applications were reported by Yu *et al*. Five distinct rotor topologies were simulated in order to analyze and compare the performance in terms of magnetic field, inductances, mechanical characteristics and short circuit performances. Rotor topologies included the V shape, U shape, VV shape, VU shape, and UU form. As a result of this research, the U shape motor delivered the best fault tolerance among all others. The study, on the other hand, proposed IPMSM motor types with 54-slot 6-pole configurations [17].

The above literature primarily aimed to investigate the impact of various topologies on IPM rotor design. However, most of the study used permanent magnet synchronous motors, and a part of the material replicated the models at speeds less than 10,000 rpm, much below the high-speed range. Thus, this paper aimed to analyze and investigate three different rotor topologies of interior permanent magnet BLDC (IPM-BLDC) for a rated speed of 30,000 rpm with 6-slot 4-pole configurations. To determine performance, the inside rotor was modelled and simulated by using the FEM. The models were compared and chosen for fabrication activities based on the induce voltage profiles and cogging torque. There are five sections presented in this paper. The first section is for introduction, next section is IPM-BLDC basic structure, the third section covering on motor sizing of IPM-BLDC, section four is analysis on rotor structure by using FEM analysis and measurement verification and the last section, is for conclusion.

2.   BASIC STRUCTURE OF IPM-BLDC FOR HIGH-SPEED ELECTRIC MOTOR

The design process began with the modelling of an IPM motor, with a focus on three basic structures of internal type rotor deemed suitable for high-speed operation. Figure 2 depicts the fundamental construction of a BLDC internal rotor. The stator is slotted, the rotor is interior permanent magnet types while the magnet is incorporated inside the rotor core. Three types of rotor structures were chosen and modelled in this work to determine the best structure to meet the high-speed criterion. Three designs were chosen based on typical IPM rotor structure. Figure 3 shows the three types of IPM rotor: a) conventional IPM radial type (C-IPM), b) hybrid V-IPM (HV-IPM), and c) hybrid IPM radial type (H-IPM).
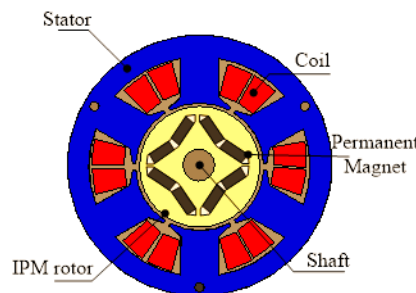

Figure 2. IPM-BLDC fundamental construction
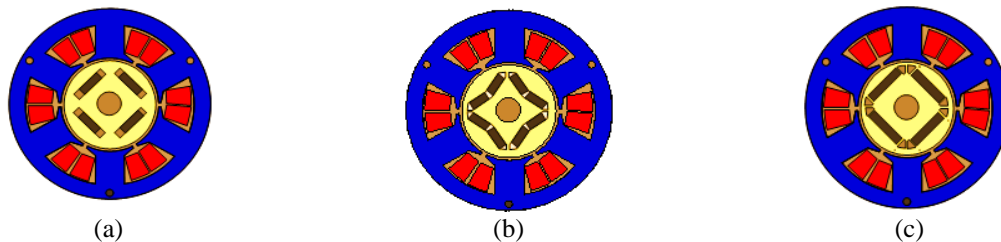

| (a) | (b) | (c) |

Figure 1. IPM BLDC model structure: (a) conventional IPM radial (C-IPM), (b) hybrid V (HV-IPM),
and (c) hybrid IPM radial (H-IPM)

The simulation for all three structures was performed in Ansys Maxwell FEM software that available in the laboratory. The Ansys Maxwell FEM software was used because it able to predict the characteristic of the back EMF and cogging torque [18]–[20]. Finally, the best rotor configuration was chosen to be fabricated in further research. In essence, the motor with higher speeds produced a low torque for the same power rating. The design criteria are shown in Table 1. The exterior diameter of each model was

set as a comparison to evaluate the performance of each model. Each model was represented with the same slot and pole number with a fixed volume of 7200 At due to available size of permanent magnet in laboratory. The permanent magnet had the same size and shape for all rotor structures.

Table 1. Design specifications

Design specifications	Value
Power, P [W]	600
No. phases	3
Rated speed range, N_r[rpm]	30,000
Maximum current, I_{max} [A]	10

3. MOTOR SIZING OF IPM-BLDC

The analysis of IPM-BLDC is illustrated in the flowchart shown in Figure 4. There are three stages to achieve the objective of work. The first stage is design and modeling stage. This involved motor sizing and rotor selection for high-speed BLDC motor. There are three selections of IPM rotors. The rotor selection is slotted type (C-IPM), hybrid V-shaped (HV-IPM) and hybrid IPM radial (H-IPM). Next stage is FEM analysis which is to evaluate the performance of model in terms of induce voltage and cogging torque evaluation. The last stage is the experimental and validation section. Here, the suitable performance of BLDC motor in FEM analysis is chosen for fabrication. The experiment and validation were carried out to ensure that the simulation and actual performance were consistent.
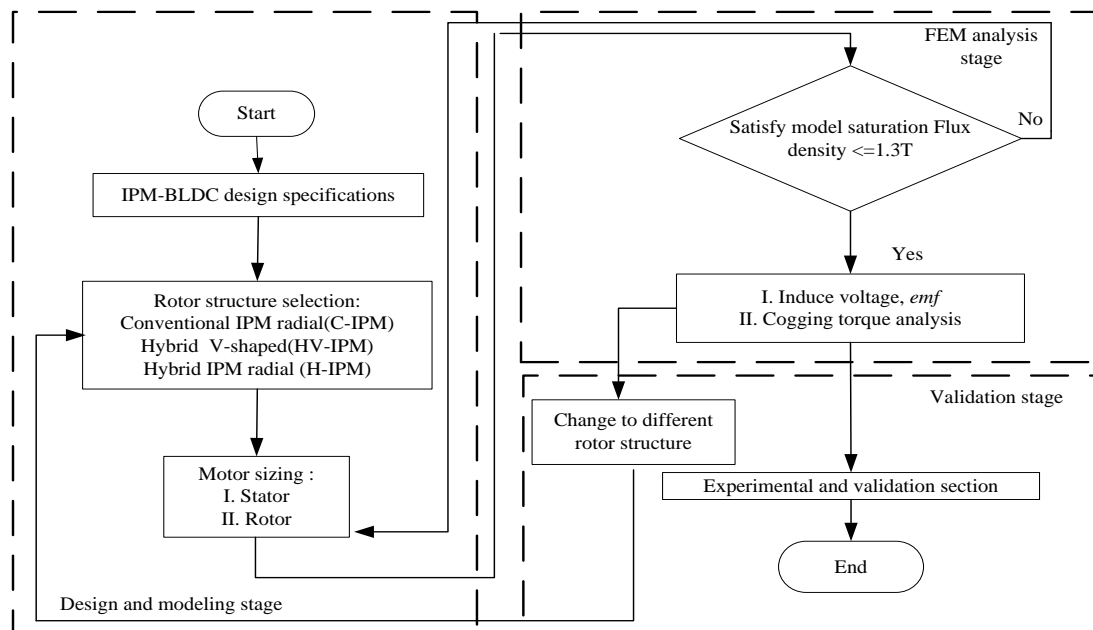

Figure 4. IPM BLDC motor design flowchart

The design of stator sizing is illustrated in Figure 5. Figure 5(a) and Figure 5(b) show the stator sizing and stack length overview. Figure 5(c) is stator flux density area. Figure 5(d) show the rotor sizing overview. Overall dimension for model IPM-BLDC was determined by using the analytical and optimal split ratio method [21]–[26]. The stator outside diameter was limited to 84 mm as fixed parameter for the model. The rotor bore was evaluated by using an optimal split ratio, λ shown in (1). The split ratio was derived from electromagnetic torque, T equation of three phase permanent magnet motor in (2). Based on (3), S_{br} is the stator bore diameter, R_{od} is rotor bore diameter, l_a is active stack length and N_{ph} represents turn windings. I_a is the RMS of the phase current and ϑ_g is the air gap flux density. The feasible range of split ratio was limited by the structure of motor. The maximum split ratio depended on the air gap length and flux density ratio, γ when the outer diameter was fixed. The flux density ratio was calculated by using (4). As a result, the ideal split ratio range for determining rotor bore was 0.45-0.75. The air gap, g was set to 1 mm, and the motor worked optimally in approximately 1 mm.

$$\lambda = \frac{R_{od}}{S_{br}} \tag{1}$$

$$T = \frac{3\sqrt{2}}{2} S_{id} l_a N_{ph} I_a B_g \tag{2}$$

$$S_{br} = \lambda R_{od} + 2l_a \tag{3}$$

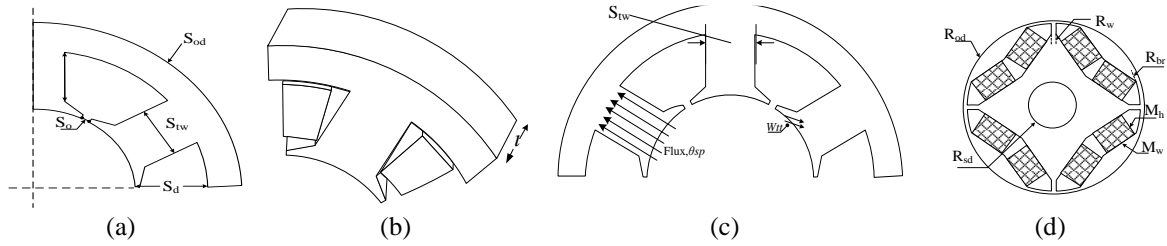$$\gamma = \frac{\vartheta_g}{B_{max}} \tag{4}$$

Figure 5. Motor sizing: (a) stator sizing, (b) stack length, (c) stator flux density area, and (d) rotor sizing

Area of tooth body, θ_{sp} was calculated by using (5). B_g was assumed to be 0.58 T and l_a was set to 30 mm. N_s which is number of stator slot was set at 6. The saturation value of stator flux density, B_{sat}, was adjusted at 1.3 T to establish the stator tooth width, St_w. Thus, the stator tooth width, S_{tw} was computed by using (6).

$$\theta_{sp} = B_g \frac{2.\pi.Sa_{id}}{N_s} \tag{5}$$

$$S_{tw} = \frac{\theta_{sp}}{B_{sat}l_a} \tag{6}$$

The entire flux traveling through the body will be divided in half in the stator teeth as shown in Figure 5(c). The flux will enter the stator yoke from the right and left sides. To complete the stator part dimension, in (7) was used. S_{id} is stator inner diameter, S_{br} is stator bore diameter, S_{tw} is stator tooth width, S_{tt} is stator tooth tang height, and S_d is slot depth. W_{tt} is stator tooth tang width, φ_x is portion flux enter from permanent magnet to the stator tooth teeth pole. Next, to calculate the stator yoke thickness, S_{yt}, in (8) was applied after the stator inner diameter was defined. Later, the slot-depth was calculated by using (9) to (12).

$$S_{id} = \left(\frac{R_{od}}{2}\right) - \left(\frac{S_{tw}}{2}\right) \tag{7}$$

$$S_{yt} = S_{od} - S_{id} \tag{8}$$

$$\varphi_x = \left[\frac{\left(\frac{2.\pi S_i}{N_s}\right) - S_{tw}}{2}\right] B_g l_g \tag{9}$$

$$W_{tt} = \frac{\varphi_x}{B_{sat}l_a} \tag{10}$$

$$S_{tt} = S_{br} + W_{tt} \tag{11}$$

$$S_d = S_{i_d} + S_{tt} \tag{12}$$

$$N_{ph} = \frac{w_c}{d_c} \times \frac{h_c}{d_c} \times \text{coil factor} \tag{13}$$

$$R_c = \rho\left(\frac{L}{A_c}\right) \tag{14}$$

The final step in the design stage is to determine the permanent magnet and rotor sizes. The size of the permanent magnet was limited according to the available size in the laboratory. The size used was 5 mm x 3 mm. The M_w x M_h is the width and thickness of the permanent magnet. The permanent magnet material utilized was Neodymium Boron Iron. The outside diameter of rotor was calculated next to the rotor size by appropriately dividing the ratio to match the typical magnet size available. Therefore, the scale of the rotor was calculated equal to half of the stator outer diameter. Each of rotor bridge and rotor web were fixed to 1 mm thickness to ensure it had same conditions for HV-IPM and H-IPM models. Considering the winding arrangements, the number of windings turns, N_{ph}, in (13) was used to assess the value. The value of w_c is approximate the coil width area, while h_c is approximate height of coil area. w_c and h_c is illustrated in Figure 6(a). The coil diameter was set to 0.7 mm due to the maximum allowable current in the motor which is 10 A. In this work, slot fill factor was assumed to be 60% of full stator slot geometry. The motor winding configurations is concentrated end winding as shown Figure 6(b). Generally, all parameters calculated is listed in Table 2.
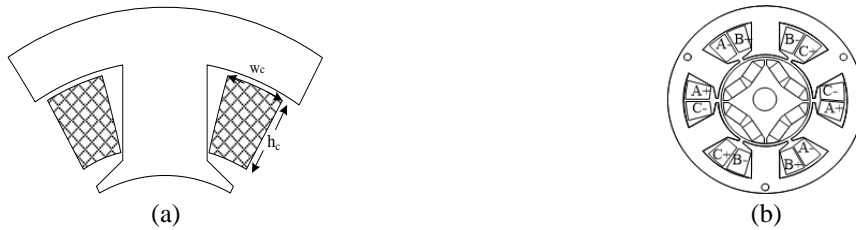

Figure 6. Winding turn and winding configurations: (a) winding turn and (b) winding configurations

Table 2. IPM-BLDC rotor design

Parameter	Rotor configurations		
	C-IPM	HV-IPM	H-IPM
Rotor external diameter [mm], R_{od}		38	
Rotor bridge [mm], R_{br}		1	
Rotor web [mm], R_w		1	
Shaft diameter [mm], R_{Sd}		10	
Magnet size, M_w x M_h [mm]		3 x 5	
Stator tooth height [mm], S_{th}		15	
Stator tooth width [mm], S_{tw}		12	
Slot opening [mm], S_o		1	
Stator outer diameter [mm], S_{od}		84	
Winding turns		30	
Air Gap [mm], g		1	
Stack length, ℓ [mm]		30	

4. FEM SIMULATION AND ANALYSIS

This section discussed the simulation result analysis, which compared all three IPM models. The models were simulated by using Ansys Maxwell FEM analysis. The performance of models was evaluated by using transient magnetic solver to define the response in time domain. The internal time step was set based on rated speed. The simulation results then compared to select the best IPM rotor structure. The cogging torque and induce voltage analysis were carried out without any current excitation of the phase windings. The model rotated according to the rated speed at 30,000 rpm. The phase resistance was ignored, and the model was assumed to be in ideal condition. The cogging torque was computed by using (15). Where, Φ_g is air gap flux, while R is air gap reluctance. Meanwhile, the induce voltage, *back emf* was computed by using (16) to compare the profiles.

$$T_{\text{cog}} = -\frac{1}{2} \Phi_g^2 \frac{dR}{d\theta} \text{ [Nm]} \tag{15}$$

$$back\,emf = N \frac{d\varphi}{dt} \text{ [V]} \tag{16}$$

The aim of comparing the simulation results is to find the induce voltage that close to trapezoidal shape that is suitable for inverter driving signal, such as six-step commutation signal. The value of induce voltage also must be in the acceptable range. In terms of cogging torque, low cogging torque value was the best with the motor allowed to operate with minimum vibration during a real operation. The following

Figure 7 shows the results of induce voltage and cogging torque for all models of IPM rotor. Referring to induce voltage simulation results in Figure 7(a), HV-IPM rotor had a good profiles that really close to trapezoidal form while the C-IPM model and H-IPM model produced a sinusoidal induce voltage. In terms of induced voltage level, H-IPM had the highest induce voltage as compared to other models. All models had a relatively modest cogging torque that fell in the mili-Newton metre (mN.m) range. As indicated in Figure 7(b), H-IPM had the lowest cogging torque, followed by HV-IPM and eventually C-IPM, which had a larger cogging torque. Based on this finding, the HV-IPM rotor structure was chosen for fabrication. The measurement results for the constructed motor are shown in the next section for validation.
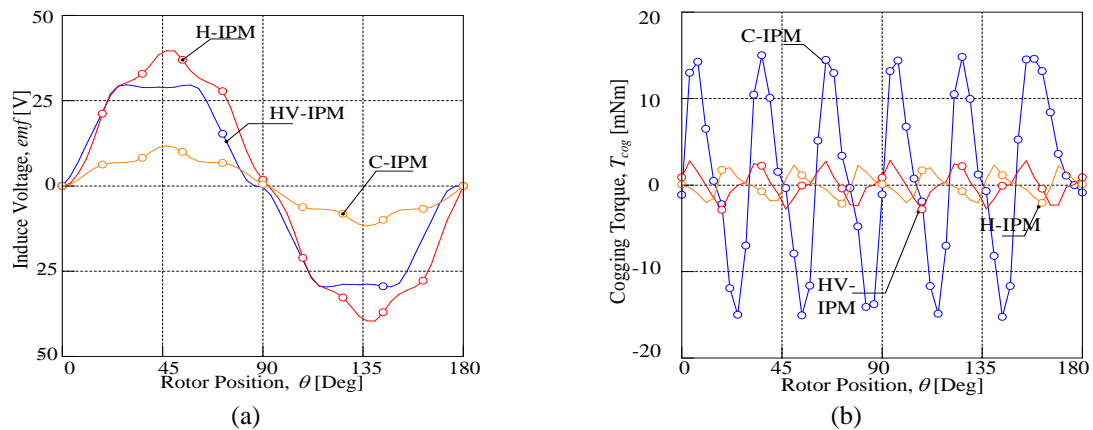
Figure 7. FEA analysis of three IPM-BLDC rotor structure: (a) induce voltage profile and (b) cogging torque

4.1. Measurement result

HV-IPM rotor shown in Figure 8 had been fabricated and assembled before ready to be tested in the laboratory. Figure 8(a) shows the cross-sectional view of an IPM BLDC motor. This prototype was covered with end cap for both sides and the stator were in the middle without stator casing as shown in Figure 8(b). A bench test was conducted to validate that the design could be implemented and to assess the findings. The goal of the bench test was to verify the induce voltage profile and establish HV-IPM ability to accomplish the rated speed. The test was conducted by rotating the prototype with a constant rotation to let the motor running at constant speed.
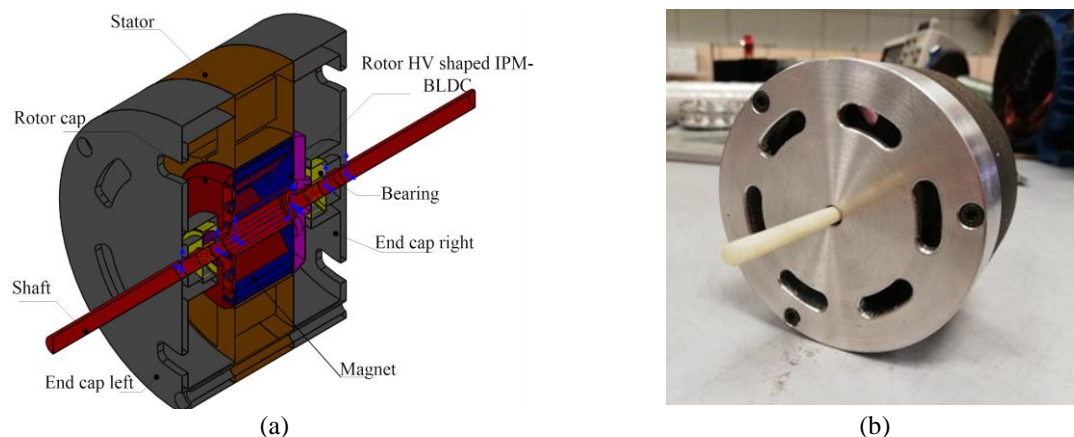

Figure 8. HV-IPM motor: (a) cross sectional view and (b) assemble prototype

Afterwards, the motor was tested by using a basic variable speed driver to check whether the rotor can operate at high speeds or otherwise. The completed prototype with a test bench setup is shown in Figure 9(a). It showed the prototype was attached with the circuit driver for a speed test evaluation. The motor running at 16 V voltage supply with 0.12 A current. The speed recorded about 14,000 rpm. Figure 9(b) is the test bench to evaluate the induce voltage. The HV-IPM BLDC was rotated constantly to produce the profiles of induce voltage. The result was captured by using an oscilloscope and compared to the simulation

results. Figure 10(a) shows the induce voltage profile for three phase HV-IPM BLDC and Figure 10(b) is the comparison between measurement and simulation for one phase. According to the results, the shape of induce voltage was relatively constant between phases, with the highest value being slightly less than the simulation value. This may be due to the saturation on stator pitch and slotting effect of stator surface. Through the results, it showed that induce voltage profile from the measurement result had a good agreement with the simulation results.
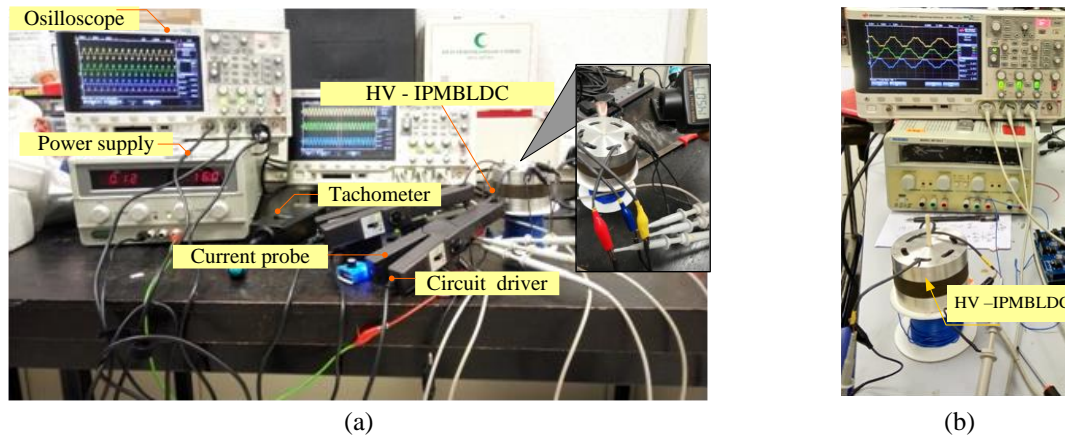
Figure 9. Test bench: (a) experimental setup and (b) test bench for induce voltage
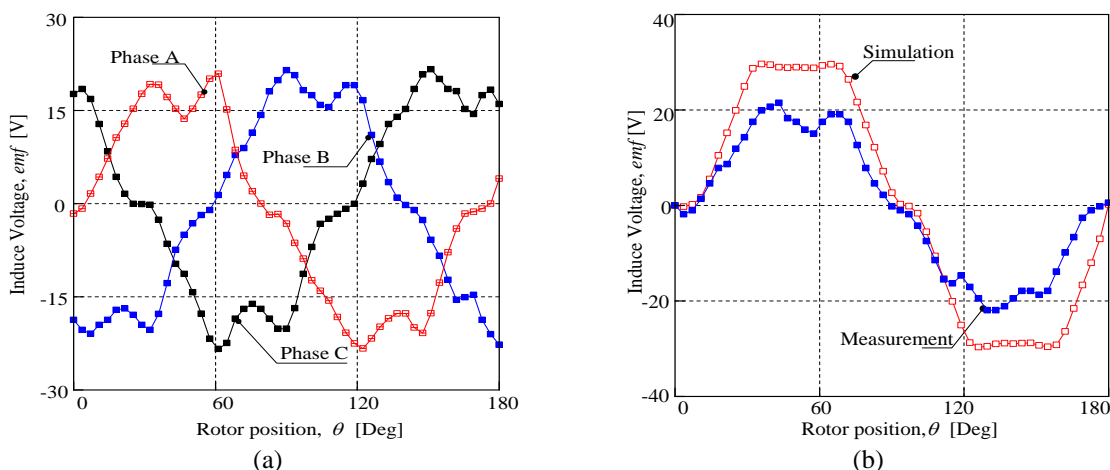
Figure 10. HV shaped IPM-BLDC test bench result: (a) three phase EMF and (b) phase a induce voltage profiles simulation and measurement comparison

5. CONCLUSION

In conclusion, the rotor type IPM motor structure for type HV IPM-BLDC had successfully designed for High-Speed Electric Motor. The design of the motor could produce speed of 14,500 rpm and fulfil the design restrictions. From the FEM analysis, the output motor can proceed at any rotor position to achieve the performance in terms of low cogging torque and induce voltage. The findings showed that the model met the design specifications and had good correlation FEM methods measurement results of hardware experimental. Thus, this result will be used as a reference and proceed to next test bench for further work.

REFERENCES

[1]   Y. B. A. Apatya, A. Subiantoro, and F. Yusivar, "Design and prototyping of 3-phase BLDC motor," in *2017 15th International Conference on Quality in Research (QiR) : International Symposium on Electrical and Computer Engineering*, Jul. 2017, pp. 209–214. doi: 10.1109/QIR.2017.8168483.

[2]   K. H. Kim, H. Il Park, S. M. Jang, D. J. You, and J. Y. Choi, "Comparative Study of Electromagnetic Performance of High-Speed Synchronous Motors with Rare-Earth and Ferrite Permanent Magnets," *IEEE Transactions on Magnetics*, vol. 52, no. 7, 2016, doi: 10.1109/TMAG.2016.2532901.

[3]   D. Gerada, A. Mebarki, N. L. Brown, C. Gerada, A. Cavagnino, and A. Boglietti, "High-speed electrical machines: Technologies, trends, and developments," *IEEE Transactions on Industrial Electronics*, vol. 61, no. 6, pp. 2946–2959, 2014, doi: 10.1109/TIE.2013.2286777.

[4]   J. Bae, Y. Jo, J. W. Ahn, and D. H. Lee, "A novel speed-power control scheme of a high speed BLDC motor for a blender machine," *2017 20th International Conference on Electrical Machines and Systems, ICEMS 2017*, 2017, doi: 10.1109/ICEMS.2017.8056147.

[5]   T. P. Banerjee, J. Roychoudhury, S. Das, and A. Abraham, "Hybrid intelligent predictive control system for high speed BLDC motor in aerospace application," *Proceedings - 3rd International Conference on Emerging Trends in Engineering and Technology, ICETET 2010*, pp. 258–262, 2010, doi: 10.1109/ICETET.2010.48.

[6]   J. Shen, X. Qin, and Y. Wang, "High-speed permanent magnet electrical machines — applications, key issues and challenges," *CES Transactions on Electrical Machines and Systems*, vol. 2, no. 1, pp. 23–33, 2020, doi: 10.23919/tems.2018.8326449.

[7]   W. Purwanto, H. Maksum, T. Sugiarto, Risfendra, A. Baharudin, and Marno, "Optimal design of stator slot geometry for high-speed spindle induction motor applications," *2019 International Conference on Information and Communications Technology, ICOIACT 2019*, pp. 811–816, 2019, doi: 10.1109/ICOIACT46704.2019.8938493.

[8]   R. R. Moghaddam, "High speed operation of electrical machines, a review on technology, benefits and challenges," *2014 IEEE Energy Conversion Congress and Exposition, ECCE 2014*, pp. 5539–5546, 2014, doi: 10.1109/ECCE.2014.6954160.

[9]   R. Dutta, K. Ahsanullah, and F. Rahman, "Cogging torque and torque ripple in a direct-drive interior permanent magnet generator," *Progress In Electromagnetics Research B*, vol. 70, no. 1, pp. 73–85, 2016, doi: 10.2528/PIERB16072001.

[10] S. X. Chen, T. S. Low, and J. P. Yang, "The Robust Design Approach For Reducing Cogging Torque In Permanent Magnet Motors," pp. 343–343, 2005, doi: 10.1109/intmag.1998.742610.

[11] G. Jiao and C. D. Rahn, "Field weakening for radial force reduction in brushless permanent-magnet DC motors," *IEEE Transactions on Magnetics*, vol. 40, no. 5, pp. 3286–3292, 2004, doi: 10.1109/TMAG.2004.832989.

[12] P. Champa, P. Somsiri, P. Wipasuramonton, and P. Nakmahachalasint, "Initial rotor position estimation for sensorless brushless DC drives," *Proceeding of International Conference on Electrical Machines and Systems, ICEMS 2007*, pp. 508–512, 2007, doi: 10.1109/ICEMS12746.2007.4412015.

[13] A. Wang, Y. Jia, and W. L. Soong, "Comparison of five topologies for an interior permanent-magnet machine for a hybrid electric vehicle," *IEEE Transactions on Magnetics*, vol. 47, no. 10, pp. 3606–3609, 2011, doi: 10.1109/TMAG.2011.2157097.

[14] H. Hao, J. Shen, C. Yuan, and Q. Qu, "Influences of machine structure on high speed PM BLDC motor," *2014 17th International Conference on Electrical Machines and Systems, ICEMS 2014*, pp. 3309–3312, 2014, doi: 10.1109/ICEMS.2014.7014063.

[15] W. Purwanto, Risfendra, D. Fernandez, D. S. Putra, and T. Sugiarto, "Design and comparison of five topologies rotor permanent magnet synchronous motor for high-speed spindle applications," *International Journal of GEOMATE*, vol. 13, no. 40, pp. 148–154, 2017, doi: 10.21660/2017.40.02765.

[16] M. H. Hwang, J. H. Han, D. H. Kim, and H. R. Cha, "Design and Analysis of Rotor Shapes for IPM Motors in EV Power Traction Platforms," *Energies*, vol. 11, no. 10, 2018, doi: 10.3390/en11102601.

[17] D. Yu, X. Y. Huang, Y. T. Fang, and J. Zhang, "Design and comparison of interior permanent magnet synchronous traction motors for high speed railway applications," *Proceedings - 2017 IEEE Workshop on Electrical Machines Design, Control and Diagnosis, WEMDCD 2017*, pp. 58–62, 2017, doi: 10.1109/WEMDCD.2017.7947724.

[18] A.J. Ali, A.H. Ahmed and B.M. Saied, "Cogging torque mitigation for PMSM using stator slots design and Magnets skewing," *2019 2nd International Conference on Electrical, Communication, Computer, Power, and Control Engineering (ICECCPE)*. Mosul, Iraq,2019, pp. 240-245, doi:10.1109/ICECCPCE46549.2019.203781.

[19] S. Raj, R. Aziz, and M. Z. Ahmad, "Influence of pole number on the characteristics of permanent magnet synchronous motor (PMSM)," *Indonesian Journal of Electrical Engineering and Computer Science*, vol. 13, no. 3, pp. 1318–1323, 2019, doi: 10.11591/ijeecs.v13.i3.pp1318-1323.

[20] T. Nur and Herlina, "Enhancement of Cogging Torque Reduction on Inset Permanent Magnet Generator by Using Magnet Edge Shaping Method," *Proceedings of 2018 International Conference on Electrical Engineering and Computer Science, ICECOS 2018*, pp. 429–434, 2019, doi: 10.1109/ICECOS.2018.8605247.

[21] J. F. Gieras, "High speed machines," *Advancements in Electric Machines*, pp. 81–113, 2008, doi: 10.1007/978-1-4020-9007-3_4.

[22] A. Tenconi, S. Vaschetto, and A. Vigliani, "Electrical machines for high-speed applications: Design considerations and tradeoffs," *IEEE Transactions on Industrial Electronics*, vol. 61, no. 6, pp. 3022–3029, 2014, doi: 10.1109/TIE.2013.2276769.

[23] J. Feng, Y. Wang, S. Guo, Z. Chen, Y. Wang, and Z. Q. Zhu, "Split ratio optimisation of high-speed permanent magnet brushless machines considering mechanical constraints," *IET Electric Power Applications*, vol. 13, no. 1, pp. 81–90, 2019, doi: 10.1049/iet-epa.2018.5051.

[24] B. Kim, "Investigation on slot-pole combinations of a PM vernier motor with fractional-slot concentrated winding configurations," *Energies*, vol. 10, no. 9, 2017, doi: 10.3390/en10091310.

[25] J. Hendershot and T. J. E. Miller, "Design of Brushless Permanent Magnet Machines," *1st ed. Magna Physic Publishing & Oxford University Press*, pp. 65–109, 2010.

[26] Y. Liu, Z. Zhu, C. Gan, S. Brockway, and C. Hilton, "Comparison of optimal slot/pole number combinations in fractional slot permanent magnet synchronous machines having similar slot and pole numbers," *The Journal of Engineering*, vol. 2019, no. 17, pp. 4585–4589, 2019, doi: 10.1049/joe.2018.8202.

BIOGRAPHIES OF AUTHORS

Nurfaezah Abdullah ⓘ 🔍 SC ◐ was born in Kuala Lumpur. She had received B.Eng. in Power Electronics and Drives in 2012 and M.Sc. Electrical Engineering at University Technical Malaysia Melaka. Currently, she is pursuing her PhD at University Technical Malaysia Melaka. Her research interests include the field in machine design, photovoltaic system, and power electronics. She can be contacted at email: faezah_abdullah@ymail.com.

Kasrul Abdul Karim ⓘ 🔍 SC ◐ received the M.Sc. from University of Bradford and Ph.D. degrees from the University of Nottingham, UK, in 2003 and 2011, respectively. He is currently associate professor at Faculty of Electrical Engineering, University Technical Malaysia Melaka, Durian Tunggal, Malaysia. His research interests include electrical machine design, power electronics, and electric vehicle. He can be contacted at email: kasrul@utem.edu.my.

Raja Nor Firdaus Kashfi Raja Othman ⓘ 🔍 SC ◐ received B.Eng., M.Sc. and PhD in Electrical Engineering from University Putra Malaysia in 2006, 2009 and 2013, respectively. He is currently associate professor in Department of Power Electrical Engineering, Faculty of Electrical Engineering, University Technical Malaysia Melaka. His research interest is applied magnetics, electrical machines, magnetic sensor and drives. He can be contacted at email: norfirdaus@utem.edu.my.

Auzani Jidin ⓘ 🔍 SC ◐ received the B. Eng., M. Eng. and Ph.D. degrees in power electronics and drives from University Technology Malaysia, Johor Bahru, Malaysia, in 2002, 2004, and 2011, respectively. He is currently a Senior Lecturer with the Department of Power Electronic and Drive, Faculty of Electrical Engineering, University Technical Malaysia Melaka, Melaka, Malaysia. His research interests include the field of power electronics, motor drive systems, field-programmable gate array, and DSP application. He can be contacted at email: auzani@utem.edu.my.

Tole Sutikno ⓘ 🔍 SC ◐ is a lecturer, and serves as the head of the Electrical Engineering Department, as well as the head of the Master Program of Electrical Engineering within the Faculty of Industrial Technology at Universitas Ahmad Dahlan (UAD) in Yogyakarta, Indonesia. In 1999, 2004, and 2016, he graduated with a Bachelor of Engineering from Universitas Diponegoro, a Master of Engineering from Universitas Gadjah Mada, and a Doctor of Philosophy in Electrical Engineering from Universiti Teknologi Malaysia. All three degrees are in the field of electrical engineering. Since the year 2008, he has held the position of Associate Professor at the Universitas Ahmad Dahlan in Yogyakarta, Indonesia. He is among the top 2% of researchers named by Stanford University and Elsevier BV as the most influential scientists in the world for 2021–present. His research interests include the areas of digital design, industrial applications, industrial electronics, industrial informatics, power electronics, motor drives, renewable energy, FPGA applications, embedded systems, artificial intelligence, intelligent control, digital libraries, and information technology. He can be contacted at email: tole@te.uad.ac.id.